*Journal of Marine Research, 55,* 353–381, 1997

# Effect of a freshwater pulse on mesoscale circulation and phytoplankton distribution in the lower St. Lawrence Estuary

**by Claude Savenkoff[1], Alain F. Vézina[1] and Yves Gratton[2]**

ABSTRACT

As part of a multidisciplinary program to study the physical-biological interactions regulating carbon flows in the lower St. Lawrence Estuary (LSLE), three cruises were conducted in June–July 1990 during a neap-spring tidal cycle when biological production was expected to be maximal. Nutrient (nitrates and silicates), phytoplankton biomass (chlorophyll), oxygen, temperature, salinity, and current fields were used to elucidate the effect of a freshwater pulse produced by the discharge of the St. Lawrence and Saguenay rivers on the current fields and the biological variability and productivity of the LSLE. A simple Rossby adjustment model is presented to explain the temporal (3–5 days) and spatial (40–50 km) scales of motion in our study region (impact of the freshwater pulse on the circulation). Prior to the passage of the pulse during the neap tide, the circulation was dominated by a downstream outflow and phytoplankton blooms were limited to areas of weak baroclinic currents downstream and along the south shore. The arrival of the pulse during the tidal transition led to the intensification of a transverse current that most likely reduced flushing and allowed phytoplankton biomass to develop further upstream and toward the north shore. During the spring tide, lower salinity waters and the bloom spread along the north shore as the transverse current weakened. Based on these observations, a new conceptual model of mesoscale physical-biological interactions in the LSLE is presented that emphasizes the importance of transverse motions in regulating mesoscale patterns in phytoplankton blooms.

## 1. Introduction

Estuaries are highly diverse environments, ranging from large deep fjords to shallow tidal creeks. They also have unique circulations, complex bathymetries, large horizontal and vertical gradients of properties, and distinct temporal dynamics at the seaward and riverine boundaries. The large variation in chemical and biological characteristics of estuaries complicates the development of paradigms and conceptual models (Sinclair *et al.,* 1981; Monbet, 1992; Vézina *et al.,* 1995). Among the unresolved problems are the control and regulation of phytoplankton biomass and production (Boynton *et al.,* 1982; Nixon and Pilson, 1983; Cloern, 1987, 1991; Cloern *et al.,* 1989; Vézina *et al.,* 1995) and the supply and recycling of nutrients (Boynton *et al.,* 1982; Malone *et al.,* 1986). Moreover, responses

1. Department of Fisheries and Oceans, Canada, Maurice Lamontagne Institute, P.O. Box 1000, Mont-Joli, Québec, G5H 3Z4, Canada.
2. INRS-Océanologie, 310 Allée des Ursulines, Rimouski, Québec, G5L 3A1, Canada.

to nutrient inputs differ from estuary to estuary, from segment to segment within a given estuary, and temporally within any segment of an estuary (Bertine *et al.,* 1979; Queguiner and Treguer, 1986; Fisher *et al.,* 1988; Wafar *et al.,* 1989).

Short-term variability in phytoplankton biomass in these systems is generally associated with changes in vertical stratification (Sinclair *et al.,* 1981). Stability of coastal waters is controlled by the balance between buoyancy flux (from surface heating or freshwater inflow) and dissipation of kinetic energy by wind and tidal mixing (Cloern, 1984). Vertical mixing of the water column (destabilized phase) is mainly caused by tides, winds, and thermohaline convection while the main stabilizing agents of the upper water column are air-ocean heat exchanges and fresh or brackish water plumes (Legendre and Demers, 1985). This one-dimensional view has been successful for explaining many features of the spatio-temporal variability of phytoplankton in estuaries and is particularly appropriate for small to mid-sized estuaries.

In large-scale estuarine systems, however, rotational effects (e.g. Coriolis forces) come into play and lead to complicated circulation patterns (e.g. unstable waves, eddies) that can have a strong influence on the zonation and activity of marine planktonic organisms (Angel and Fasham, 1983). The lower St. Lawrence Estuary (hereafter termed the LSLE) is an example of a large-scale estuary. Its width (30 to 50 km), equal to several internal Rossby radii, is sufficient to allow development of lateral instabilities and mesoscale eddies. Indications of cross-shore currents and eddies have been reported repeatedly (Ingram and El-Sabh, 1990; Mertz and Gratton, 1990). Vézina *et al.* (1995) described a cross-shore front forming in late June coincident with a phytoplankton bloom and two separate occurrences of a cyclonic pattern spreading across the estuary. Correlations of physical variables with phytoplankton biomass and nutrient variables were maximal during these events. Therefore, these mesoscale structures appear critical in shaping and regulating phytoplankton blooms in the LSLE.

Estuarine dynamics are strongly influenced by fortnightly ($M_f$: 14.8 days) and semidiurnal ($M_2$: 12.4 hours) tidal components (Legendre and Demers, 1985; Monbet, 1992). Production cycles have been mainly linked to the fortnightly spring-neap tidal cycle in the LSLE (Sinclair, 1978) and other estuaries and coastal embayments (Sinclair *et al.,* 1981; Harrison *et al.,* 1991). In light-limited and nutrient-rich estuaries, productivity is expected to fall during spring tides, when vigorous mixing reduces the average light field experienced by phytoplankton, and rise toward neap tides, when increased stratification allows utilization of the resuspended nutrients (Sinclair, 1978; Demers *et al.,* 1979; Demers and Legendre, 1981). However, Vézina *et al.* (1995) did not observe spatially-averaged biomass minima at spring tides and maxima near neap tides. In fact, they provided evidence that mesoscale physical-biological structure fluctuated on a scale of 3–5 days, faster than the spring-neap cycle.

The study of Vézina *et al.* (1995) lacked the temporal resolution and the information on currents that was needed to elucidate the hydrodynamic processes responsible for these fluctuations. In this paper, we use a more complete set of physical-biological observations

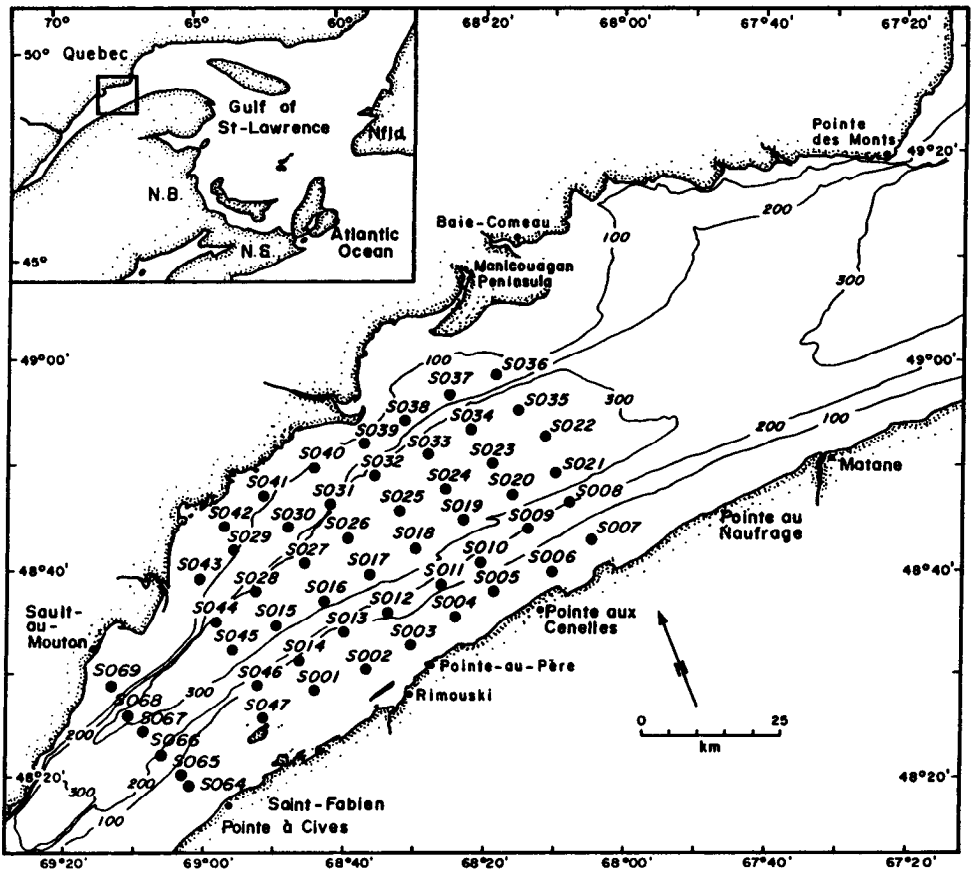


Figure 1. Station grid and bathymetric map of the study site.

than the previous studies to elucidate the effect of eddy motions on the biological variability and productivity of the LSLE: data were collected on three cruises over a summer neap-spring tidal cycle (June–July 1990). We compare mesoscale nutrient (nitrates: $NO_3$; silicates: $SiO_4$), phytoplankton biomass (CHL), and oxygen (OXY) fields to temperature (TEMP), salinity (SAL), and current fields. We show that a transverse current, associated with a low salinity anomaly traveling down the estuary, determined the timing and location of a summer phytoplankton bloom. We suggest that this current accounts for mesoscale patterns in the production of the LSLE.

## 2. Materials and methods

### *a. Study site*

Our study concerns an area of the St. Lawrence Estuary between Pointe à Cives—Sault-au-Mouton and Pointe au Naufrage—Baie-Comeau (Fig. 1). The St. Lawrence Estuary

begins at the end of the St. Lawrence River drainage system, at the landward limit of the saltwater intrusion near Île d'Orléans, and extends about 400 km seaward to Pointe-des-Monts, where its channel opens into the Gulf of St. Lawrence (Fig. 1). The estuary is subdivided on the basis of bathymetry and hydrographical features as follows: the upper estuary, with large tides and low salinities extending from Île d'Orléans to the confluence of the St. Lawrence and the Saguenay rivers, exhibits uneven topography ranging from shallow plateaus to deep channels (over 100 m deep); the lower estuary, stretching from the Saguenay to Pointe-des-Monts, is much deeper (up to 350 m), with a comparatively smooth bottom.

The LSLE is an elongated channel with an average length, width, and depth of 200 km, 40 km, and 300 m, respectively. Fresh waters enter the LSLE from the upper St. Lawrence Estuary and the Saguenay River at the upstream end and from the North Shore rivers (Manicouagan Peninsula) at the downstream end. Because of Coriolis effects, this freshwater discharges principally along the southern side of the estuary, eventually forming the Gaspé Current, a strong, narrow, and often unstable coastal jet that runs along the Gaspé Peninsula. To counteract this outward flow, salt water moves upstream, along the 350-m deep Laurentian Trough that runs the whole length of the LSLE. These waters are periodically upwelled by the tides at the head of the Laurentian Channel, near the confluence with the Saguenay River, where the bottom shoals from 300 m to 50 m over 20 km (Forrester, 1974; Ingram, 1975; Greisman and Ingram, 1975; Therriault and Lacroix, 1976). Using satellite observations, Gratton *et al.* (1988) showed that the head of the Laurentian Trough is cold regardless of the phase of the $M_2$ and fortnightly tidal cycles, suggesting that strong mixing processes are at work there. The strength of these mixing processes varies with the tidal cycle. Their interactions with the brackish flows from the upper estuary and the Saguenay largely control the downstream properties of the surface waters in the LSLE (Ingram, 1979).

*b. Cruises*

Three cruises were conducted between 29 June (Day 180) and 12 July 1990 (Day 193) in the subarea of the LSLE (Fig. 1). During each cruise, a grid of 50 stations with an alongshore grid spacing of 10 km and a cross-shore grid spacing of 7 km was visited. The 10 km alongshore spacing is also an absolute upper bound on the semidiurnal tidal excursion (6.2 hours times 0.40 m $s^{-1}$). The grid was covered as quickly as possible to minimize aliasing effects. Each cruise began at station 69 in the northwest corner and proceeded along the cross-shore lines. The whole grid was generally completed in three days (Table 1), while each section was usually covered in less than six hours.

Aanderaa current meters were moored simultaneously at seven locations between May and September 1990 (Fig. 2): two moorings at the head of the Laurentian Channel (L2 and L3) and five in the study area (T1 to T5). We will present data from the instruments moored at 20 m depth.

Meteorological and tidal conditions over the sampling period are presented in Figure 3.

Table 1. Cruises over the study area during June–July 1990. Column abbreviations are as follows: *n* stations gives the number of stations at which $CTDO_2$ casts and pump profiles of *in vivo* fluorescence and nitrate and silicate concentrations were attempted; *n* TS, *n* CHL, *n* $NO_3$, *n* $SiO_4$, and *n* OXY give the number of CTD, calibrated fluorescence, nitrate, silicate, and dissolved oxygen profiles that were retained for this study. Lastly, the dates of the first and last stations for each cruise are given.

| Cruise | *n* stations | *n* TS | *n* CHL | *n* $NO_3$ | *n* $SiO_4$ | *n* OXY | First station yy/mm/dd (hh:mm) (day of the year) | Last station yy/mm/dd (hh:mm) (day of the year) |
|---|---|---|---|---|---|---|---|---|
| neap | 55 | 48 | 44 | 26 | 22 | 48 | 90/06/29 (01:30) (Day 180) | 90/07/03 (02:55) (Day 184) |
| transition | 54 | 52 | 49 | 42 | 28 | 52 | 90/07/03 (20:50) (Day 184) | 90/07/06 (20:40) (Day 187) |
| spring | 48 | 47 | 48 | 46 | 36 | 45 | 90/07/07 (05:00) (Day 188) | 90/07/09 (22:30) (Day 190) |
| All | 157 | 147 | 141 | 114 | 86 | 145 | | |

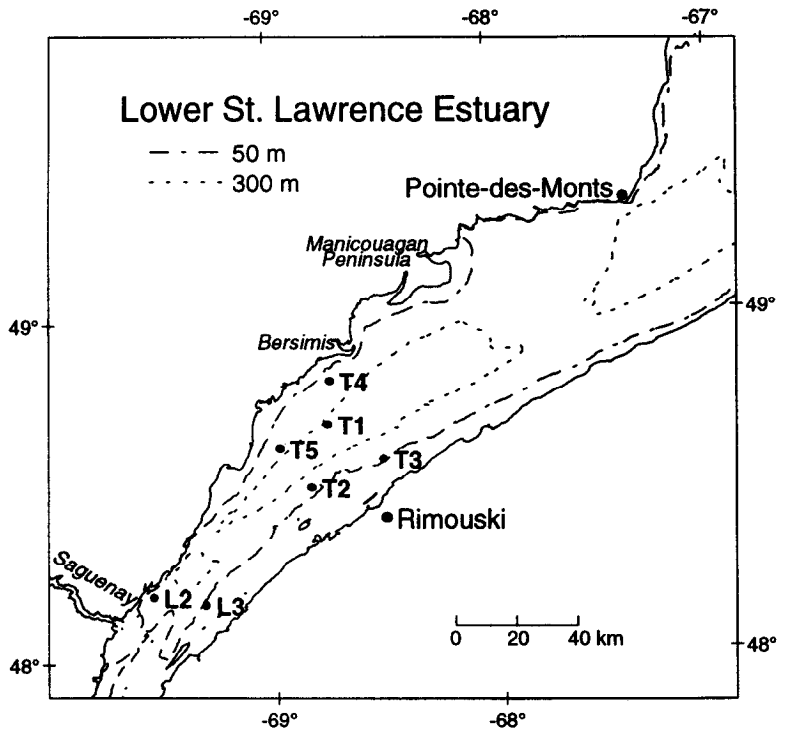


Figure 2. Mercator map of the lower St. Lawrence Estuary showing the mooring locations and the 50 and 300 m isobaths. Moorings L2 and L3 were located at the head of the Laurentian Channel while moorings T1 to T5 were in the study area.

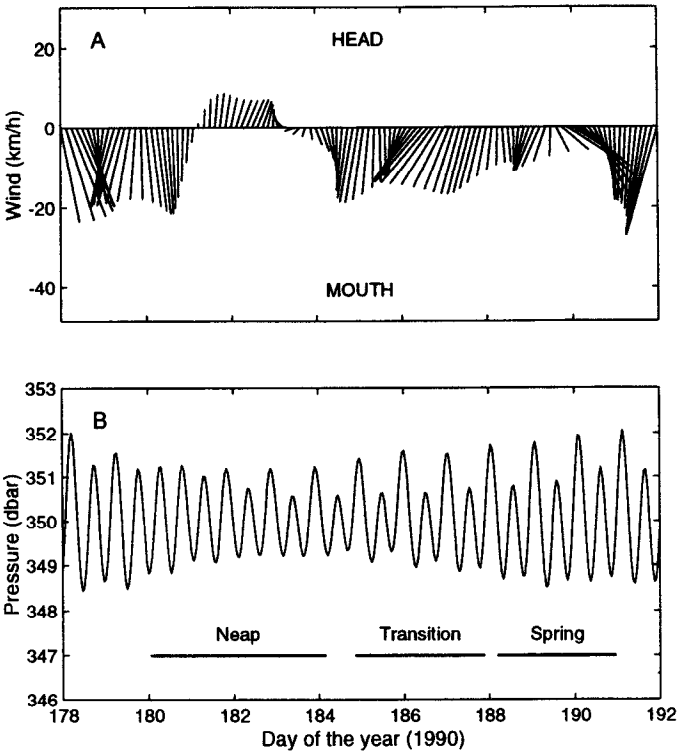


Figure 3. (A) Wind stick diagram (in km $h^{-1}$). Downward wind vectors indicate an alongshore (toward the mouth) wind orientation. (B) Bottom pressure (in dbar) in the center of the study region (mooring T1: see Fig. 2 for location). One decibar (dbar) is equivalent to an elevation of one meter.

Meteorological conditions (Fig. 3A) were generally sunny and winds tended to be weak, 20 km $h^{-1}$ or less. The wind changed direction from upstream at the beginning of the sampling period to downstream a few days later and decreased in intensity afterward. The three cruises covered a neap-spring tidal cycle (Fig. 3B; Table 1). Finally, Figure 4 presents the daily freshwater discharges of the main upstream (upper panel) and downstream (lower panel) tributaries over the same period as the current moorings were in place. The freshwater pulse described in this study is believed to originate from the discharge of the Saguenay River (Laforêt, 1994).

*c. Measurements on station*

At each station, temperature, salinity, density, oxygen, and turbidity profiles were determined down to 5–10 m off-bottom with a multiparametric Applied Microsystem STD-12 instrument. Vertical profiles of the horizontal currents were also obtained along each cross-shore section with a 150 kHz Acoustic Doppler Current Profiler (ADCP).

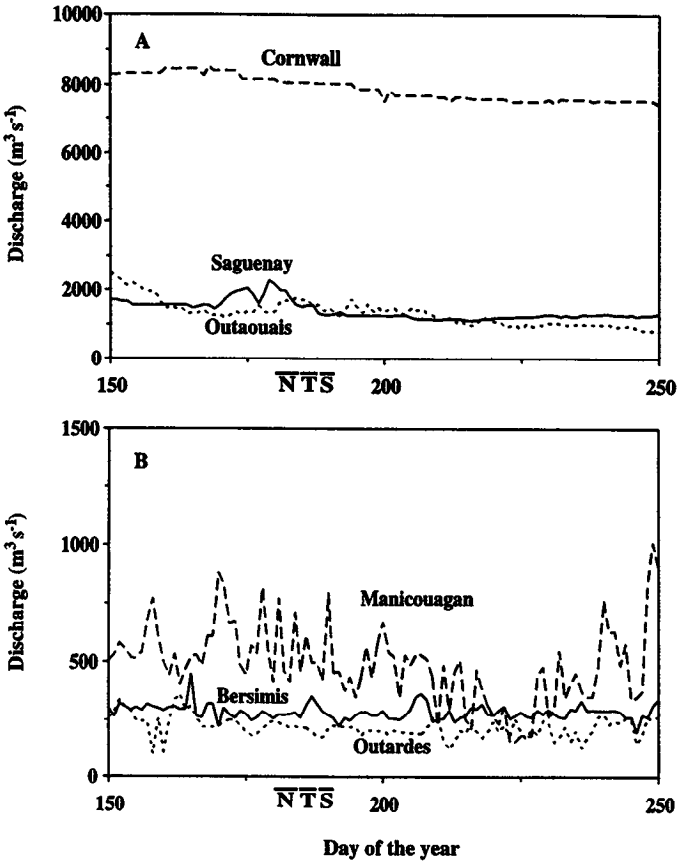


Figure 4. Daily freshwater discharge (in $m^3 s^{-1}$) of the main tributaries of the lower St. Lawrence Estuary: (A) the St. Lawrence River at Cornwall, the Outaouais River and the Saguenay River. (B) The north shore rivers: Bersimis, Manicouagan and Outardes. N: neap tide; T: transition from neap to spring tide; S: spring tide.

A submersible pump (Jacuzzi), equipped with a pressure sensor and a light probe (Photosynthetically Available Radiation meter, PAR; Licor), was lowered gradually over the top 30 m of the water column (or to the bottom at shallow stations) for biological and chemical profiling. Pumped water was routed through a fluorometer (Turner model 10) and a Technicon Autoanalyzer II set up for nitrate and silicate analysis. The pump was lowered at ca. 2 m $min^{-1}$ to allow time for the nutrient signals to develop in the Technicon (Anderson and Okubo, 1982). Nutrient (nitrate and silicate) concentrations were determined by standard automated methods on a Technicon Autoanalyzer II (Parsons *et al.*, 1984). Blanks and standards were run through the Technicon every six hours on average to calibrate the instrument. The outputs of the sensors and the laboratory instruments were recorded continuously on a data logger (Campbell Scientific) and stored on computer disks.

Samples from the pump outflow were taken regularly (every three stations or three hours on average) for calibration of the fluorometer. The samples were filtered immediately over Whatman GF/F glass fiber filters and frozen for later analysis on land. The chlorophyll determinations, performed no later than one month afterward, followed Strickland and Parsons (1972), except that the grinding step was omitted.

During each cruise, a number of biogeochemical and physical parameters were measured from top to bottom at three stations located in the Laurentian Trough (stations 67, 26, and 23) (Savenkoff *et al.,* 1995a, b). We used samples collected with 12 l Niskin bottles from up to eleven depths over the entire water column during daytime to calibrate the continuously-measured data (e.g. CTD-oxygen calibration). The depths sampled were usually as follows: depths where 50, 10, and 1% of the surface incident radiation remained (euphotic zone, defined as extending to the depth where 1% of the surface light remains); 25, 50, 70, 90, and 110 m (intermediate water); and 150, 200, 250, and, station depth permitting, 300 and 320 or 340 m (deep water). Dissolved oxygen concentration was determined according to the Winkler method as described by Aminot and Chaussepied (1983). Samples from three optical depths (50, 10, and 1% of the surface irradiance) were collected for cell identification and biomass (chlorophyll) and primary production determinations. Samples for microplankton counts were fixed with iodine Lugol solution at 2% v/v final concentration and placed in a 50 ml settling chamber. All phytoplankton cells were counted and identified using the Utermöhl inverted microscope technique (Lund *et al.,* 1958) modified by Blasco (1971). Primary production was determined by the $^{14}C$ method as described in Vézina *et al.* (1995).

*d. Data processing*

The ADCP was programmed to record one minute ensemble averages of the horizontal velocity vertically averaged over 8 m, starting at 10 m. Therefore, the first measurement represents the mean velocity between 10 and 18 m. The vertical velocity shear was obtained by averaging between five and ten consecutive one-minute absolute horizontal velocity vertical profiles before removing the mean vertical velocity and linearly interpolating every 2.5 km. Since the ADCP was measuring the horizontal velocities on and between stations, the lateral resolution was already approximately 2.5 km. The time series from the moored instruments were filtered to remove the energy at periods less than one hour and re-sampled every hour; a low pass (25 h) tidal filter was then applied to the hourly data. The CTD data were linearly interpolated at every meter.

Fluorescence and nutrient readings for every meter were obtained by averaging neighboring readings ($\pm 0.5$ m). These averaged readings were transformed to chlorophyll, nitrate, and silicate profiles using extracted chlorophyll measurements ($n = 127$, $r^2 = 0.51$, $P < 0.001$) and shipboard standards for the nutrients. We calculated the calibrated oxygen value using the relationship between the oxygen measured with the STD-12 and those determined by the Winkler method ($n = 90$, $r^2 = 0.93$, $P < 0.001$). Calibrated fluores-

cence, silicate, nitrate, and oxygen profiles were integrated over the euphotic zone. These integrated values were used to compute the spatial distribution of these parameters.

*e. Objective classification of physical and biological profiles*

The variability in the vertical profiles of temperature (TEMP), salinity (SAL), calibrated fluorescence (CHL), nitrate ($NO_3$), silicate ($SiO_4$), and dissolved oxygen (OXY) was synthesized into groups of profiles with similar vertical distributions of properties using the method described in Vézina *et al.* (1995). Briefly, the data were decomposed into Empirical Orthogonal Functions (EOF; better known as Principal Components in the biological literature) that represent major features in the vertical profiles (e.g. depth-averaged center of mass, stratification, subsurface maxima or minima). This method regroups the large number of vertical profiles measured during sampling surveys into a limited number of classes based on similarities in shape, hopefully unrelated to the stages of the semi-diurnal tidal cycle.

Clustering algorithms were then applied to regroup the amplitudes (or loadings) of each variable into a limited number of groups. We calculated the EOFs on the normalized data matrix using the MATLAB SVD procedure (MATLAB, 1992) and used the K means algorithm (Wilkinson, 1992) to cluster the loadings. This clustering method maximizes the ratio of inter- to intra-cluster variance (Hartigan, 1975) and is roughly analogous to a one-way analysis of variance where groups are unknown and the largest $F$ value is sought by reassigning members to each group (Wilkinson, 1992, p. 31). We used the SYSTAT program (Wilkinson, 1992) to generate separate analys s assuming that there were either 2, 3, 4, or 5 clusters of loadings. We retained the number of clusters that produced the largest $F$-ratios for the loadings of the different variables.

## 3. Results

*a. Variations in physical, chemical and biological properties during the neap-spring tidal cycle*

Over the whole study period (11 days), there was a net shift from cooler and more saline surface waters toward warmer and fresher surface waters. Mean surface and euphotic zone temperatures increased from 8.0 to 9.6°C and from 6.9 to 8.3°C, respectively, while mean surface and euphotic zone salinities decreased from 26.7 to 24.3 and 27.0 to 25.2, respectively (Table 2). The haline and thermal stratifications, defined as the change in these variables between the sea surface and the 1% light level (12 m), increased from the neap to spring tide. Chlorophyll and dissolved oxygen integrated over the euphotic zone increased from the neap to spring tide, concurrent with decreases in integrated nitrate and silicate concentrations (Table 2).

Pairwise Spearman correlations between physical and biological/chemical properties were weak (Table 3). For the combined cruises, CHL, $NO_3$, and $SiO_4$ variations were correlated to euphotic zone temperature but not to euphotic zone salinity or to any measure

Table 2. Mean (±standard deviation) and range (in parentheses) of the surface physical, chemical, and biological properties for each cruise. Temperature, salinity, chlorophyll *a*, nitrate, silicate, and oxygen values were integrated over the euphotic zone (0–12 m). Integrated temperature and salinity values were then divided by the thickness of the euphotic layer (12 m). The difference in the physical values over the euphotic zone (to 12 m; the depth where 1% of the surface incident radiation remained) was used as an index of stratification.

| | Neap | Transition | Spring |
|---|---|---|---|
| surface temperature (°C) | 8.0 ± 1.7 | 8.4 ± 0.8 | 9.6 ± 1.3 |
| | (5.5–12.3) | (5.5–9.7) | (6.1–12.5) |
| euphotic zone temperature (°C) | 6.9 ± 1.3 | 7.9 ± 0.9 | 8.3 ± 1.5 |
| | (4.4–9.9) | (4.2–9.4) | (4.5–10.9) |
| thermal stratification (°C) | 2.1 ± 1.5 | 1.3 ± 1.1 | 3.0 ± 1.7 |
| | (0.0–7.2) | (0.0–4.6) | (0.3–6.5) |
| surface salinity | 26.7 ± 0.7 | 25.2 ± 1.2 | 24.3 ± 1.3 |
| | (24.6–28.5) | (22.7–28.0) | (22.6–26.5) |
| euphotic zone salinity | 27.0 ± 0.7 | 25.6 ± 1.2 | 25.2 ± 1.4 |
| | (26.0–28.8) | (22.8–28.6) | (23.1–28.1) |
| haline stratification | 0.9 ± 0.7 | 1.1 ± 0.7 | 2.2 ± 1.0 |
| | (0.1–4.2) | (0.0–2.7) | (0.3–4.3) |
| chlorophyll *a* (mg $m^{-2}$) | 19 ± 16 | 20 ± 11 | 27 ± 19 |
| | (6–57) | (3–48) | (8–84) |
| nitrate (mmol $m^{-2}$) | 154 ± 83 | 119 ± 50 | 104 ± 42 |
| | (11–288) | (3–180) | (7–181) |
| silicate (mmol $m^{-2}$) | 197 ± 65 | 194 ± 66 | 153 ± 79 |
| | (1–284) | (45–350) | (15–331) |
| oxygen (mmol $m^{-2}$) | 3806 ± 94 | 3866 ± 72 | 3885 ± 77 |
| | (3559–3992) | (3684–3997) | (3699–4009) |

of stratification. CHL levels at any station or during any cruise tended to be higher in water masses of higher temperature, with concomitant drops in $NO_3$ and $SiO_4$. Spatial variations in CHL and nutrients could be related to temperature stratification during the neap tide and to euphotic zone salinity during the neap and transition tide periods (Table 3).

The lowest three EOFs were found to explain 51% of the total variation and were retained for the classification of vertical structure groups; retaining more EOFs did not substantially change the classification. No single group was related to a particular stage of the tidal cycle: each group contained profiles from high, low, flood, and ebb tides. The first three EOFs yielded 18 amplitude coefficients (6 variables times 3 EOFs) for each station of each cruise. We developed separate groups for the physical profiles (temperature, salinity, and dissolved oxygen; T-S-O) and the biological profiles (calibrated fluorescence, nitrate, and silicate; F-N-Si). This reflects the low correlations between physical and biological properties observed during the cruises (Table 3).

*b. Physical-biological structures during the neap-spring tidal cycle*

*i. Mesoscale salinity and current fields.* We base our description on contours of salinity and horizontal velocity at 15 m depth. Each variable (salinity and calibrated fluorescence)

Table 3. Matrix of Spearman correlation coefficients between physical, chemical, and biological properties of the surface layer during the 1990 cruises. Temperature, salinity, chlorophyll *a*, nitrate, silicate and oxygen values were integrated from 0 to 12 m. The difference in the physical values over the euphotic zone (0–12 m; the depth where 1% of the surface incident radiation remained) was used as an index of stratification. Euphotic integrated temperature (IT) and thermal stratification (ΔT): °C; euphotic integrated salinity (IS) and haline stratification (ΔS): no unit; chlorophyll *a* (CHL): mg $m^{-2}$; nitrate ($NO_3$), silicate ($SiO_4$) and oxygen concentration (OXY): mmol $m^{-2}$. Numbers in boldface indicate significance at $P < 0.05$.

| | IT | ΔT | IS | ΔS | CHL | $NO_3$ | $SiO_4$ | OXY |
|---|---|---|---|---|---|---|---|---|
| neap | | | | | | | | |
| IT | 1.00 | | | | | | | |
| ΔT | **0.36** | 1.00 | | | | | | |
| IS | **−0.28** | **0.31** | 1.00 | | | | | |
| ΔS | **−0.32** | **0.32** | 0.24 | 1.00 | | | | |
| CHL | **0.55** | **0.53** | **0.45** | −0.22 | 1.00 | | | |
| $NO_3$ | **−0.55** | **−0.60** | **−0.56** | −0.10 | **−0.84** | 1.00 | | |
| $SiO_4$ | **−0.43** | −0.39 | −0.13 | **0.49** | **−0.49** | 0.27 | 1.00 | |
| OXY | 0.06 | **0.31** | **0.53** | 0.17 | **0.46** | **−0.42** | −0.09 | 1.00 |
| spring | | | | | | | | |
| IT | 1.00 | | | | | | | |
| ΔT | **0.38** | 1.00 | | | | | | |
| IS | **−0.68** | 0.27 | 1.00 | | | | | |
| ΔS | −0.23 | 0.25 | 0.06 | 1.00 | | | | |
| CHL | **0.51** | −0.18 | 0.12 | −0.28 | 1.00 | | | |
| $NO_3$ | **−0.41** | 0.22 | **−0.31** | 0.19 | **−0.85** | 1.00 | | |
| $SiO_4$ | **−0.43** | 0.28 | −0.22 | −0.04 | **−0.78** | **0.75** | 1.00 | |
| OXY | 0.18 | −0.15 | 0.11 | 0.07 | **0.32** | **−0.40** | −0.15 | 1.00 |

| | IT | ΔT | IS | ΔS | CHL | $NO_3$ | $SiO_4$ | OXY |
|---|---|---|---|---|---|---|---|---|
| transition | | | | | | | | |
| IT | 1.00 | | | | | | | |
| ΔT | **−0.32** | 1.00 | | | | | | |
| IS | −0.09 | **0.34** | 1.00 | | | | | |
| ΔS | **−0.32** | **0.32** | −0.02 | 1.00 | | | | |
| CHL | **0.56** | −0.01 | **0.62** | −0.19 | 1.00 | | | |
| $NO_3$ | **−0.63** | 0.16 | **−0.47** | **0.37** | **−0.86** | 1.00 | | |
| $SiO_4$ | −0.05 | −0.22 | **−0.36** | −0.18 | −0.24 | 0.07 | 1.00 | |
| OXY | −0.16 | 0.11 | 0.18 | 0.24 | 0.01 | 0.02 | 0.11 | 1.00 |
| all | | | | | | | | |
| IT | 1.00 | | | | | | | |
| ΔT | −0.07 | 1.00 | | | | | | |
| IS | **−0.54** | **0.24** | 1.00 | | | | | |
| ΔS | 0.04 | **0.43** | **−0.24** | 1.00 | | | | |
| CHL | **0.64** | 0.15 | 0.13 | −0.03 | 1.00 | | | |
| $NO_3$ | **−0.58** | −0.11 | −0.16 | 0.02 | **−0.87** | 1.00 | | |
| $SiO_4$ | **−0.48** | −0.15 | −0.06 | −0.18 | **−0.66** | **0.58** | 1.00 | |
| OXY | **0.23** | 0.11 | −0.06 | **0.31** | **0.34** | **−0.27** | −0.18 | 1.00 |

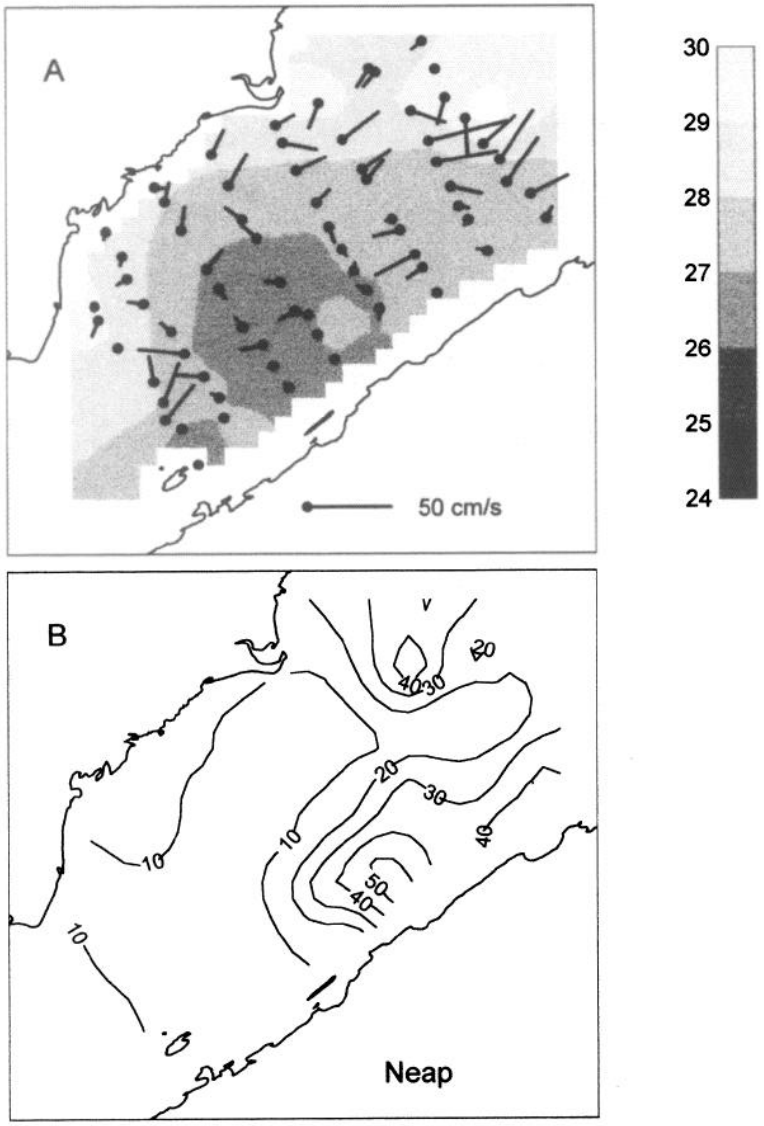


Figure 5. Spatial distribution of physical and biological parameters in the neap tide period. (A) Mean baroclinic currents between 10 and 18 m superposed on the salinity contours at 15 m. The velocity scale is in the lower right hand corner. (B) Spatial distribution of chlorophyll (calibrated fluorescence; mg $m^{-2}$) integrated over the euphotic zone.

was finely interpolated on a 5 km × 5 km grid using a kriging algorithm (Deutsch and Journel, 1992; Marcotte, 1991) and then contoured. Cross-shore transects are identified by the number of the first station on the south shore.

Figures 5, 6, and 7 present the distribution of salinity and baroclinic velocity (upper

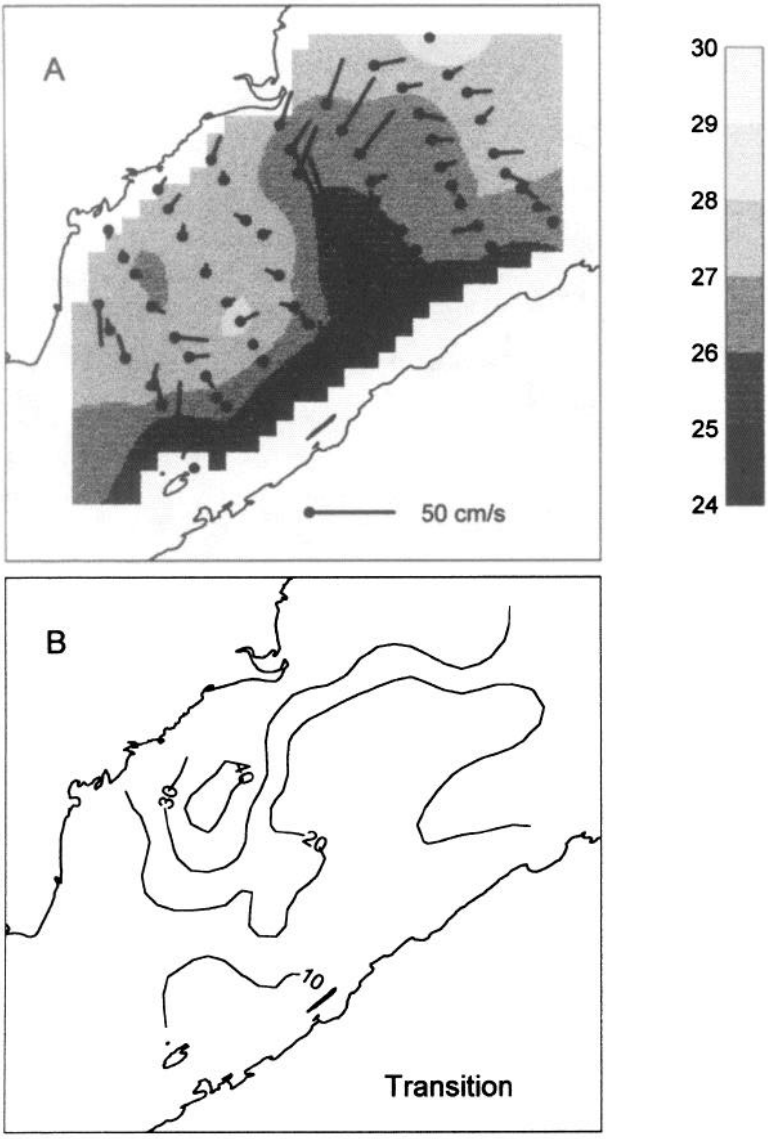


Figure 6. Spatial distribution of physical and biological parameters in the transition period. (A) Mean baroclinic currents between 10 and 18 m superposed on the salinity contours at 15 m. The velocity scale is in the lower right hand corner. (B) Spatial distribution of chlorophyll (calibrated fluorescence; mg $m^{-2}$) integrated over the euphotic zone.

panels) and chlorophyll (lower panels) for each of the three cruises. During the neap tide (Fig. 5A), the salinity distribution was characterized by a relatively low salinity water mass (27 salinity isoline) anchored on the south shore and spreading over the center of study area. Baroclinic currents were anticyclonic around the low salinity mass with a significant

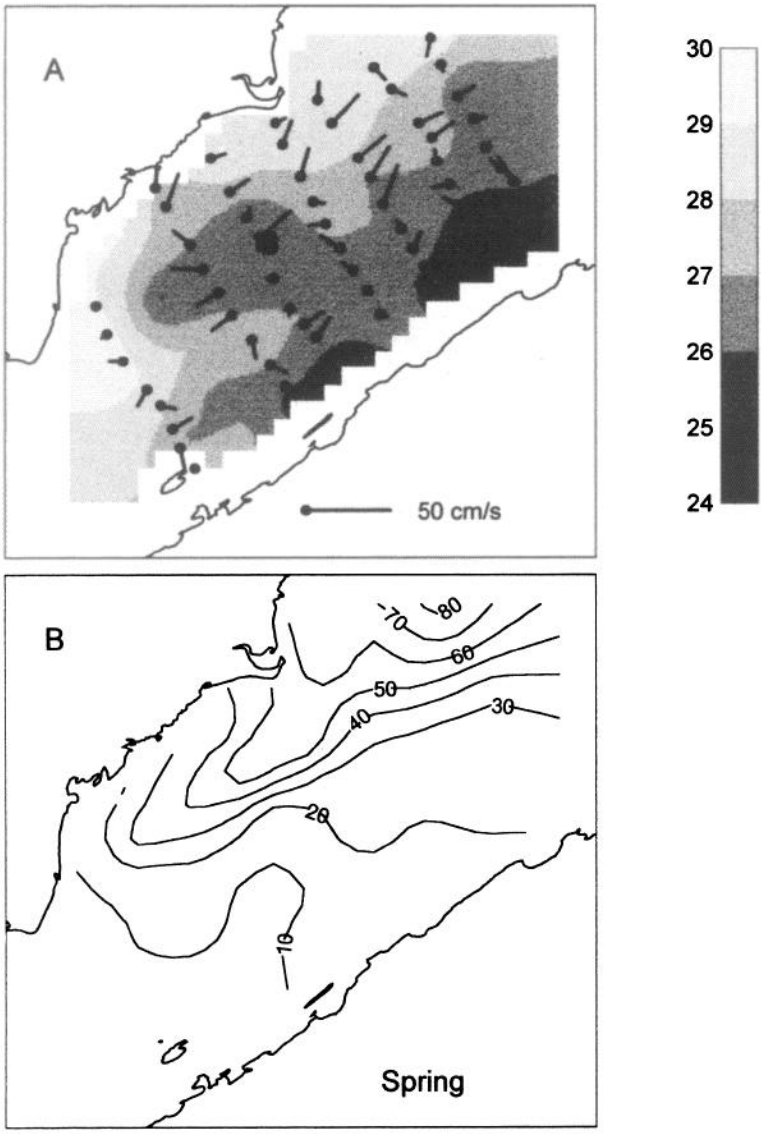


Figure 7. Spatial distribution of physical and biological parameters in the spring tide period. (A) Mean baroclinic currents between 10 and 18 m superposed on the salinity contours at 15 m. The velocity scale is in the lower right hand corner. (B) Spatial distribution of chlorophyll (calibrated fluorescence; mg $m^{-2}$) integrated over the euphotic zone.

outflow along the 28–29 isolines near the north shore and then through the middle of the estuary.

During the transition period (Fig. 6A), waters with much lower surface salinities appeared along the south shore, forming a coherent pulse-like feature across the estuary

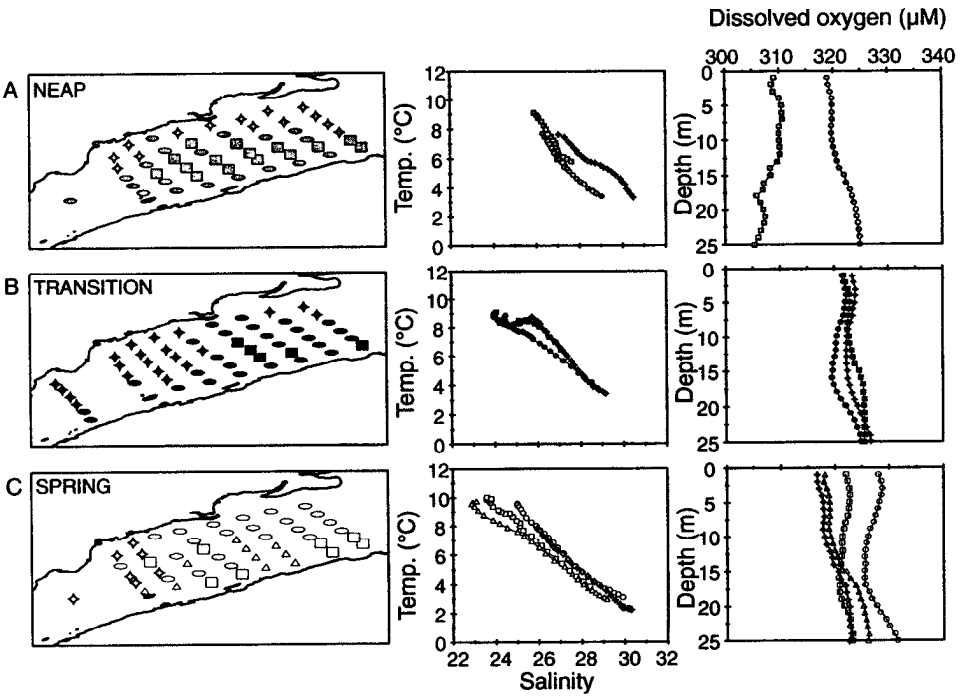


Figure 8. Major groups of physical variables (temperature, salinity, and dissolved oxygen) identified for each cruise by an objective analysis (see text) and their spatial distribution. The leftmost panels show the distribution on maps of the study area, the central panels show the *T-S* profiles, and the rightmost panels show the oxygen profiles. Each mean profile (0–25 m depth) is marked by a different symbol that is then used to locate its group on the maps. (A) neap tide cruise; (B) transition tide cruise; (C) spring tide cruise. During the neap tide, the groups identified by grey circles and stars were characterized by the same oxygen profile.

centered on transect #4. Baroclinic currents were characterized by a strong transverse current curling anticyclonically downstream of the feature.

This coherent feature disappeared during the spring tide (Fig. 7A), and waters enclosed by the 27 salinity isoline had spread more broadly over the study area. The transverse current was weaker, but there were strong baroclinic currents along the 27–28 salinity isolines, flowing downstream east of transect #4 and upstream west of transect #3.

*ii. Temperature-salinity diagrams.* We used different symbol colors (white, grey and black) for each tidal period to show that we applied the statistical analysis separately for each period. Although we cannot confirm the continuity of a group from one tidal period to another, the groups with the same symbol represent the most probable succession. The *T-S* diagrams for the neap tide distinguish among the low salinity core waters (Fig. 8A, grey squares), the saltier waters along the north shore (Fig. 8A, grey stars), and waters of intermediate salinity between the two (Fig. 8A, grey circles). The water mass that occupies the center of the estuary and the south shore (Fig. 8A, grey squares), with low salinity and

high surface temperature, was also characterized by low oxygen concentration (305–310 μM).

During the transition period, all *T-S* diagrams were fresher (shift toward the left, Fig. 8B). However, objective analysis separated three groups: one group with the strongest stratification located in the center of the feature (Fig. 8B, closed squares), another low salinity group but more mixed vertically on the periphery of the feature (Fig. 8B, closed circles), and a saltier water mass upstream of the feature (Fig. 8B, closed stars).

During the spring tide, *T-S* diagrams show strong warming and freshening over the whole area except at the upstream edge, where saltier and cooler waters were still found (Fig. 8C, open stars). The objective analysis identified three more *T-S* curves, with the saltier and least stratified profiles found mostly near the north shore (Fig. 8C, open circles) and the fresher and more stratified profiles clustered along the south shore (Fig. 8C, open squares and open triangles).

*iii. Mesoscale phytoplankton fields.* Initially, phytoplankton biomass was low over most of the area except for two patches of high chlorophyll *a* biomass located downstream and close to the north and south shores (Fig. 5B). These small blooms were associated with different water masses: the north shore bloom corresponded to saltier waters and the south shore bloom to fresher waters (Figs. 5 and 8A).

During the transition from the neap to the spring tide, the chlorophyll *a* values decreased on the south shore while they increased on the north shore (Fig. 6B). Chlorophyll fields showed a patch of high chlorophyll near the north shore, centered just upstream of the pulse-like feature (Fig. 6).

During the spring tide, a band of high chlorophyll extended parallel to the north shore, intensifying from upstream to downstream and just above the 27–28 salinity isolines (Fig. 7).

*iv. Vertical phytoplankton and nutrient profiles.* Vertical profiles of chlorophyll *a* biomass and nutrients for the two patches identified during the neap tide (Fig. 9A, grey triangles and grey circles) indicated strong biomass maxima in the top 15 m associated with nutrient minima. We determined primary production/chlorophyll (PP/B) ratios averaged for the 50 and 10% optical depths for selected stations. We obtained the highest value, a PP/B ratio of about 20 mg C mg chl $a^{-1}$ $h^{-1}$, at station 6 (grey triangle group), located in the south shore bloom, suggesting an area of active growth.

During the transition period, the patch of high chlorophyll near the north shore corresponded to strong chlorophyll maxima and nutrient minima in the top 15 m (Fig. 9B, closed diamonds). The PP/B ratios increased from the neap to transition tide in the north shore area (from 3.1 to 7.3 mg C mg chl $a^{-1}$ $h^{-1}$ at station 26 and from 6.8 to 11.5 mg C mg chl $a^{-1}$ $h^{-1}$ at station 23) and suggested the beginning of the bloom during this period. On the other hand, other areas of relatively high chlorophyll biomass downstream and within the anticyclonic cell corresponded to subsurface chlorophyll peaks (Fig. 9B, closed

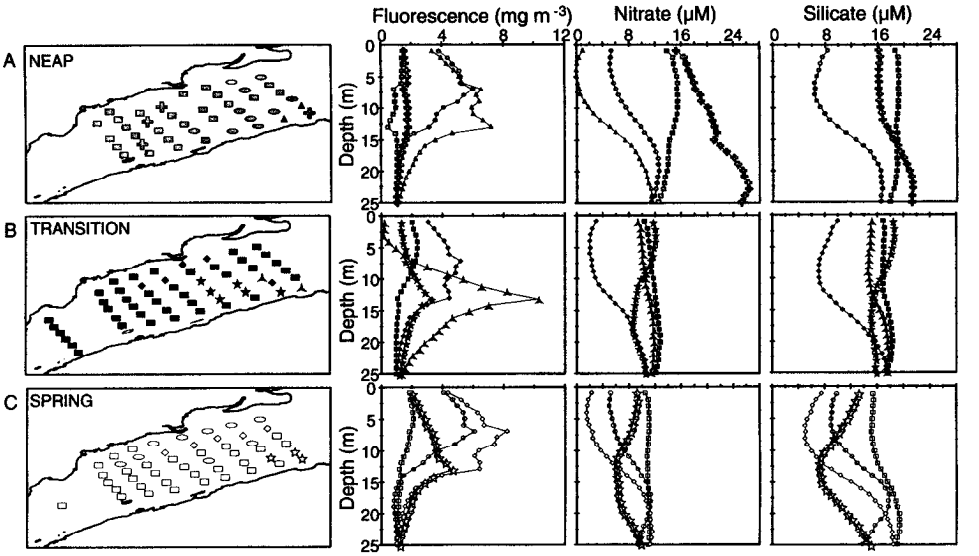


Figure 9. Major groups of biological variables (calibrated fluorescence, nitrate, and silicate) identified for each cruise by an objective analysis (see text) and their spatial distribution. The leftmost panels show the distribution on maps of the study area and the second, third, and fourth sets of panels show the calibrated fluorescence, $NO_3$, and $SiO_4$ profiles. Each mean profile (0–25 m depth) is marked by a different symbol that is then used to locate its group on the maps. (A) neap tide cruise; (B) transition tide cruise; (C) spring tide cruise. The largest nitrate concentration of the group symbolized by a cross during the neap tide could be due to a malfunction of the Technicon Autoanalyser.

chevrons and closed stars) with slight nutrient depletion at depth instead of at the surface (Fig. 9B, closed stars).

During the spring tide, the band of high chlorophyll along the north shore was close to the 27 salinity isoline (Fig. 7 and Fig. 9C, open circles and open diamonds). Subsurface chlorophyll peaks with mid-water nutrient minima were still found near the south shore at the downstream edge (Fig. 9C, open stars). The area influenced by the north shore bloom was greatest during this period. The bloom was dominated mainly by diatoms (*Thalassiosira nordenskioeldii* and other *Thalassiosira* made up 85%), in agreement with the study of Levasseur *et al.* (1984). Levasseur *et al.* (1984) showed that diatoms (size $> 20$ μm) form the bulk of the summer phytoplankton biomass in the LSLE. Diatoms are observed in the water column only during summer, from mid-June or the beginning of July until the end of September, while naked flagellates (size $< 20$ μm) are present in the water column throughout the year, with peak values reached in July and September. We found significant relationships only between diatoms and primary production ($n = 25$, Spearman's $r = 0.70$, $P < 0.001$) and diatoms and chlorophyll *a* biomass ($n = 26$, Spearman's $r = 0.69$, $P < 0.001$). No significant relationships were noted between primary production or chlorophyll *a* biomass and autotrophic dinoflagellates (e.g. *Katodinium rotundatum,*

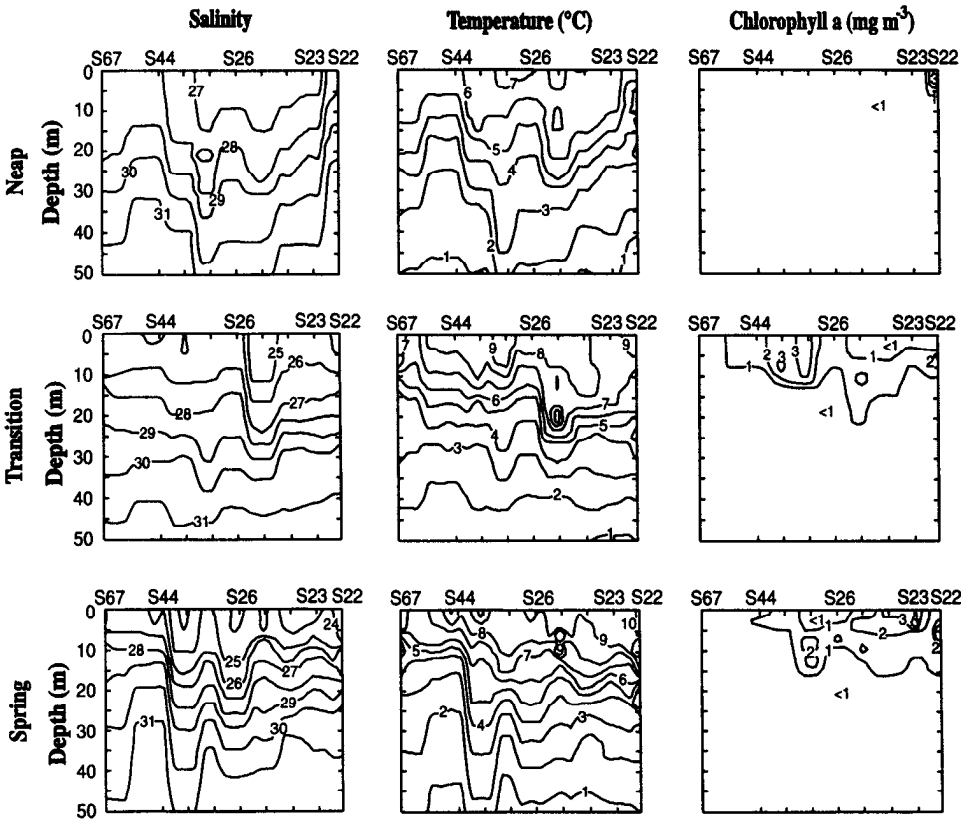


Figure 10. Vertical distributions of salinity, temperature (°C), and chlorophyll *a* concentration (calibrated fluorescence; mg $m^{-3}$) in the top 50 m of the stations located in the Laurentian Trough (see Fig. 1 for location).

*Alexandrium tamarensis, Gyrodinium aureolum*) or other autotrophs (e.g. cryptomonas species, pyramimonas species, *Mesodinium rubrum*). The PP/B ratios determined in the bloom region generally decreased from the transition to spring tide (from 7.3 to 2.2 mg C mg chl $a^{-1}$ $h^{-1}$ at station 26 and from 11.5 to 6.5 mg C mg chl $a^{-1}$ $h^{-1}$ at station 23) with the exception of station 40 (increase from 11.6 to 15.5 mg C mg chl $a^{-1}$ $h^{-1}$), which was close to the center of the bloom.

*v. Alongshore sections of salinity, temperature, and chlorophyll a concentration.* The longitudinal sections of salinity, temperature and chlorophyll *a* concentration on the alongshore line between station 67 and station 22 summarize the impact of the pulse on the vertical physical and biological structures. During the neap tide, an inverted dome in the salinity and temperature isolines was observed, consistent with an anticyclonic flow in the area at that time (Fig. 10). The generally low chlorophyll levels (<1 mg $m^{-3}$) found

throughout the area during the neap tide were also confirmed, with the exception of a small downstream concentration (Fig. 10).

During the transition period, the broad dome was replaced by a sharper low salinity spur near station 26 (Fig. 10), corresponding to the transverse current seen on the horizontal map (Fig. 6A). Chlorophyll *a* maxima were found on both sides of the feature, with a subsurface peak downstream and a surface peak upstream (Fig. 10).

During the spring tide, the section shows many small-scale oscillations in the isolines, probably reflecting the strong action of semidiurnal tides at that time. Nevertheless, we see a general upward movement of the surface salinity and temperature isolines (see the 25 and 26 isohalines and the 9°C isotherm going upstream in Fig. 10). The location of the 1 mg $m^{-3}$ chlorophyll *a* isoline was close to the 7°C isotherm during the transition and spring tides and indicated the zone of active biological activity (Fig. 10).

## 4. Discussion

Our results show that high frequency (days) unsteady motions, or eddy variability in the sense of Freeland *et al.* (1986; unresolved high frequency variance due to eddies, pulses, etc.), in estuarine circulation may be critical to the regulation and distribution of phytoplankton blooms in large estuaries like the LSLE as well as estuarine seas whose dimensions exceed their internal Rossby radius. We will first briefly review the evidence for the mesoscale perturbation that we observed, estimate its velocity, and then present a simple physical model to describe the impact of the freshwater pulse on the circulation. Then, we will suggest how this perturbation, in particular the transverse motion during the transition from the neap to spring tide, affects phytoplankton distribution and growth in the LSLE. Finally, we attempt to generalize our observations and develop a new conceptual model of mesoscale physical-biological interactions in the LSLE.

### *a. Evidence for transverse motions in the LSLE*

The presence of (northward) transverse currents in the LSLE has been inferred many times in the literature, both from observations and models. Previous studies in the LSLE have indicated that the buoyancy-induced current occasionally veers toward the north shore near Rimouski while at other times it proceeds along the south shore where it feeds the Gaspé Current (Mertz *et al.*, 1989). El-Sabh (1977) proposed that the transverse current deviates toward the north shore with two branches: one moves seaward along the north shore toward the gulf and forms a large anticyclonic gyre between Pointe-des-Monts and Île-du-Bic; the other turns west and moves upstream to form a smaller cyclonic eddy between Rimouski and Tadoussac. Vorticity considerations promote cross-channel (cyclonic vorticity) flow as the lighter water enters the progressively deeper waters of the Laurentian Channel (Mertz and Gratton, 1990). Currents recorded across the estuary near Rimouski over 20 days in 1965 (Forrester, 1967; 1970) revealed residual northward currents with speeds of 7 cm $s^{-1}$ at 10 m below the surface. Murty and El-Sabh (1977)

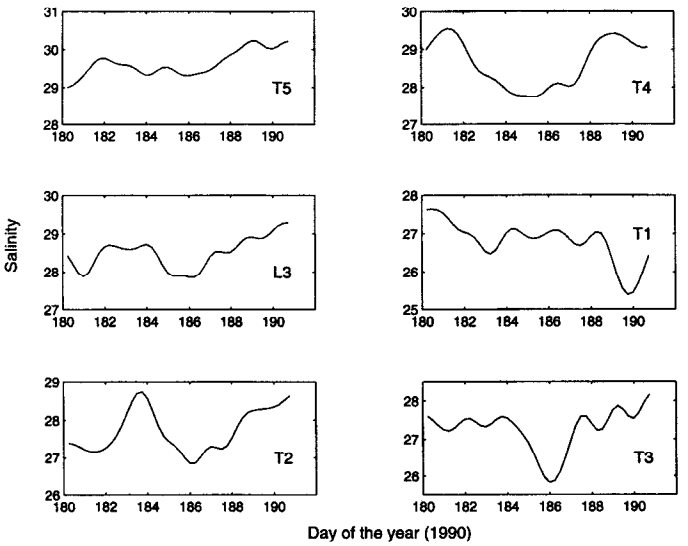


Figure 11. Low-pass (periods greater than 25 h) salinity time series at 20 m for six of the moorings shown in Fig. 2.

suggested that such a current could arise from the system's adjustment to a changing wind field while Koutitonsky *et al.* (1990) proposed an adjustment to seasonal freshwater runoff pulses. Water mass analyses in the area (El-Sabh, 1977; Therriault and Levasseur, 1985; Vézina *et al.,* 1995) indicate that isopycnals often cross the estuary toward the north shore near Rimouski. In our study, the presence of weak winds suggests that a transverse current was set up (or intensified) very quickly as soon as a lateral density gradient formed. In particular, the freshwater pulse was accompanied by a "bump" in the surface elevation. We will first determine the velocity of the freshwater pulse and then look at the adjustment of the currents to this anomaly in the surface elevation by solving the Rossby adjustment problem (Gill, 1982).

*b. Velocity of the freshwater pulse in the LSLE*

Freshwater enters the estuary from the St. Lawrence River, from the Saguenay River at Tadoussac, and from the Bersimis, Outardes, and Manicouagan rivers on the north shore of the LSLE (Manicouagan Peninsula in Fig. 1). The freshwater runoff from the St. Lawrence River produces seasonal pulses that are advected downstream by horizontal currents with a downstream reduction of the pulse's amplitude caused by mixing or entrainment of the pulse with deeper or surrounding water (Tee and Lim, 1987). Higher frequency pulses are also observed. Laforêt (1994) has shown that four freshwater pulses moved over the head region (moorings L2 and L3) between late May and early July 1990. The low-frequency salinities and trends, recorded in the surface layer (at the 20 m moorings, T1 to T5), also confirmed the presence of freshwater pulses (Fig. 11). During our study (late June to early

July, days 180 to 190), two freshwater pulses were identified in the L3 low-passed salinity data (Fig. 11; days 181 and 186) and were the last two of the discharge period (Laforêt, 1994). The lag between the pulse at L3 (day 181, Fig. 11) and T2 (day 186, Fig. 11) was five days. This yields, for a separation of 75 km, a velocity of 15 km per day or 15 cm $s^{-1}$. This value compares favorably with the lowpass currents at L3 and T2 (not shown), the so-called background velocity, which are both about 15 cm $s^{-1}$.

*c. Rossby adjustment model to explain the temporal (3–5 days) and spatial (40–50 km) scales of motion*

Geostrophy, the balance between the pressure gradient and the Coriolis terms in the equations of motion, is the steady state in an inviscid rotating system. The water will flow down the pressure gradient and will be deflected to the right (in the northern hemisphere) until the pressure gradient force exactly balances the Coriolis force. The horizontal scale of this adjustment, achieved over an inertial period (approximately 16 h at 48N), is the internal Rossby deformation radius. For a two-layer fluid, with the bottom layer at rest, this radius is given by:

$$R_i^2 = (g'H_l)/f^2 \tag{1}$$

where $g'$ is the reduced gravity, $H_1$ the thickness of the surface layer, and $f$ the inertial frequency. The reduced gravity is gravity (9.8 m $s^{-2}$) multiplied by the density difference between layers and divided by the average density. For the study region, $R_i$ is about 10 km. The surface velocity may be obtained from Margule's equation (Gill, 1982), with:

$$fv = g(\Delta h/x) \tag{2}$$

where $\Delta h/x$ is the sea-surface slope, i.e. the difference in height ($\Delta h$) over a distance $x$. A change in slope of 10 cm over 40 km will produce a velocity of 25 cm $s^{-1}$ in the lowpass velocity measured at T1 at a depth of 20 m (Fig. 12A). For comparison, the sea-surface slope across the Gulf Stream is 1 m over 100 km, which yields a velocity scale of 1 m $s^{-1}$. The low-pass sea level data at T1 (not shown), corrected for the inverse barometric effect, still showed a set of 10–20 cm troughs and crests from day 170 to day 200. A crest of about 10 cm was present on day 183 (days 181 to 185, centered on day 185).

We used the equations for the homogeneous Rossby adjustment problem (Gill, 1982) with gravity replaced by reduced gravity. The east-west sea surface slope is found in Figure 12B and the corresponding north-south geostrophic adjustment velocity is in Figure 12C. The last stick diagram (Fig. 12D) was obtained by adding an oscillating (see below) east-west velocity to the north-south geostrophic velocity. The east-west velocity at T1 was observed to oscillate between $-10$ and $+20$ cm $s^{-1}$, with a 2–4 day period, between days 170 and 195. If we add a background velocity varying linearly between $+15$ and $-15$ cm $s^{-1}$, in phase with the sea level changes of Figure 12B, to the geostrophic velocity of Fig. 12C, we obtain the velocity shown in Figure 12D. With an average drift of 15 km $d^{-1}$, the 100 km scale of Figures 12B to 12D is equivalent to the six day scale of

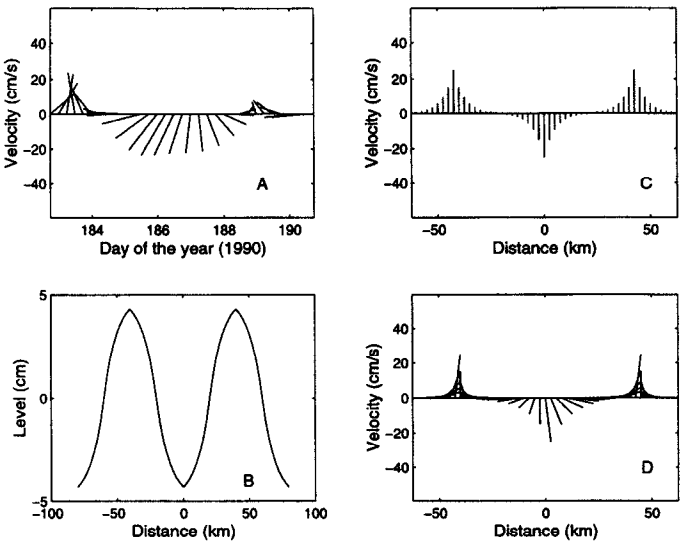


Figure 12. A simple Rossby adjustment problem for the study region: (A) low-pass velocity at 20 m depth observed at mooring T1. (B) Typical east-west oscillation of the sea surface: 10 cm over 40 km. (C) North-south geostrophic velocity corresponding to the surface slope given in panel B. (D) Final velocity obtained by adding a background velocity oscillating linearly between +15 and −15 cm $s^{-1}$, in phase with the sea level changes of panel B, to the geostrophic velocity of panel C. The spatial pattern of panel D, drifting at 15 km $d^{-1}$, could produce the time series observed at mooring T1 (panel A).

Figure 12A. Comparison of Figure 12A and Figure 12D shows that our simple Rossby adjustment model can explain the temporal (3–5 days) and spatial (40–50 km) scales of motion in our study region. The passage of a pulse would induce a southward flow that would rotate cyclonically to a northward flow within 3–5 days leaving a clockwise (anticyclonic) gyre in the downstream half of the study. This northward transverse current seems to persist until another event perturbs the system. The clockwise gyre was present at 40 m (not shown) over the the whole study period, but was intensified in the transition period.

*d. Impact of transverse motions on phytoplankton distribution*

Our results present a picture of continuously changing mesoscale physical-biological structure in the LSLE. Basically, the distribution of the biological properties from the neap to spring tide can be linked to the intensification of a transverse current associated with a freshwater pulse that arrived from the head of the Laurentian Channel. A phytoplankton bloom developed on the upstream side of the pulse in the study area then spread upstream and downstream as the pulse apparently mixed with the surrounding waters. Prior to this event, the circulation was dominated by a downstream outflow and phytoplankton blooms

were limited to the downstream edge, away from the area of stronger currents. This suggests that transverse motions are associated with phytoplankton blooms in this area.

The positive correlations between biomass and temperature could reflect an association between higher biomasses and increased residence time, allowing for surface heating and biomass accumulation. This interpretation is reinforced when the phytoplankton's spatial patterns are compared to the current fields. During the neap tide and transition periods, areas with high chlorophyll are clearly found in areas of weak baroclinic currents, either inside the low salinity region during the neap tide or outside the low salinity spur during transition. Contrary to previous studies in the LSLE and other systems (Cloern, 1984; Levasseur *et al.,* 1984; Harrison *et al.,* 1991), vertical density stratification, largely determined by salinity stratification, was not the major factor regulating bloom dynamics. The mesoscale circulation pattern was more directly involved in determining the spatial pattern of phytoplankton development.

During the transition period, the bloom appeared to originate in the region of strong horizontal shear associated with the transverse current as shown by the distribution of fluorescence-nitrate profiles and the longitudinal sections. The high surface chlorophyll values were found on the left side of the northward-flowing current, which is also the dense side of the front. This observation indicates that the patch was not advected with the buoyant freshwater flow but originated locally, as is also corroborated by the positive correlation between chlorophyll *a* and euphotic zone salinity values during the neap and transition tide periods. Surface chlorophyll maxima and localized nutrient depletion within the patch could result either from growth processes overtaking renewal by flushing in this area or from growth enhanced over the general background. High production to biomass ratios measured at a station inside the patch relative to stations outside would tend to support enhanced growth; however, data are scant and the observed differences cannot be definitely attributed to the effect of the front. Given that nutrients were available in high concentrations everywhere during the neap tide, enhanced nutrient supply by a secondary vertical circulation at the front is unlikely to explain increased growth and biomass. The presence of biomass accumulation on the less stratified side also seems to rule out a positive impact of vertical stratification on phytoplankton residence time in the surface layer and thus growth in a nutrient-rich situation. Therefore, a reduction in flushing linked to the change in baroclinic circulation seems the most likely explanation for the accumulation, although secondary cross- or along-frontal circulation could also affect the pattern of biomass accumulation.

The arrival of the pulse during the transition period also had a substantial effect on the vertical structure of phytoplankton and nutrients on the right side of the transverse current, which was also the lighter side of the water mass front. Subsurface biomass maxima and nutrient minima appeared underneath the strong halocline that formed in the region of the transverse current. This is consistent with an overflow of light surface water, trapping older surface water with its biological contents underneath. The process is more complex since

the subsurface structures actually intensified toward the spring tide, after the pulse peak. Nevertheless, this illustrates the importance of the pulse and its associated circulation in moving biological and chemical signals from the surface to depth.

The rapidity of changes in the current field explains the lack of association between vertical physical and biological structures. Lack of correlation between physical and biological structures is actually a common situation, even when the physical structure is clearly forcing biological processes. Franks (1992) has reviewed several studies of biological distributions under different types of fronts, including the type of water mass/buoyancy front observed here during the transition period, and has found no correlation between the length scales of the physical and biological patches. He argued that this is most likely due to mismatch between the temporal scales of the front and those of the biological processes that determine growth and biomass accumulation. The time scale of circulation changes in our study (3–5 days) is faster than the estimated 5–10 days needed by phytoplankton to respond to and equilibrate with a new physical regime. Therefore, the lack of correlation between biological and physical variables should not be interpreted to mean that the physical event did not cause the biological response, although it certainly complicates the task of demonstrating causality.

The other impact of transverse motion is to inject buoyancy from the south shore, where the freshwater outflow of the St. Lawrence-Saguenay rivers is normally confined, to the north shore. This in turn enhances the vertical stability of the north shore's generally more saline and weakly stratified waters. The increased vertical stability is noticeable during the spring tide when lower salinity and more stratified waters were spread along the north shore and over a much greater area than during the previous two cruises. As a result, high biomass and low nutrient levels were much more widely distributed, leading to higher regional production during spring tides. This led to a sequence of high production along the south shore during neap tides followed by high production along the north shore during spring tides. This transverse motion could represent another mechanism by which the neap-spring tidal cycle can influence production in the LSLE.

The biological importance of episodic transverse motions has been noted in other estuarine systems. In south San Francisco Bay, Huzzey *et al.* (1990) showed that a background pattern of weak, non-tidal circulation can be disrupted in coastal plain estuaries by tidal, meteorological, or hydrologic forcings at the event scale. Such events may be characterized by enhanced flows that modify the horizontal and vertical salinity distributions and generate cross-channel flows that persist for several days and coincide with large-scale redistributions of phytoplankton biomass. Malone *et al.* (1986) demonstrated similar connections between lateral transports and phytoplankton distribution across upper Chesapeake Bay. The sequence of phytoplankton blooms and subsequent increases in bacterial abundance appeared to be initiated by lateral advection and upwelling of bottom water rich in ammonium and phosphate (Malone *et al.*, 1986).

*e. Generalization of the mesoscale physical-biological patterns observed*

Previous workers have tried to surmise the effect of recirculation in the Rimouski area on phytoplankton and production processes. Sinclair (1978) conducted a 5-d survey of the LSLE during July 1975 (17–21 July, neap tide). He found a strong cross-channel gradient in biomass, with higher levels along the south shore. This gradient paralleled the salinity and temperature gradient of the surface layer with warmer and less saline water along the southern shore. Moreover, he found that the temporal distributions of phytoplankton observed in front of Rimouski were not caused by different types of water being advected past the station in a west-east direction, but were representative of a temporal sequence within a water mass. These fluctuations paralleled the distribution of surface water stratification, and the regularity of the fluctuations suggested that the distributions were controlled by the cyclic variability in the magnitude of tidal mixing following the neap-spring cycle. Sinclair proposed that his observations were due to the residual clockwise gyre in the surface water, which had been proposed by El-Sabh (1977). The increased residence time of the surface water would tend to reduce the advective losses from the region, thus permitting the higher biomass levels observed and the maintenance of a relative homogeneity in species composition. This would be consistent with a repetition, possibly over successive neap-spring cycles, of the sequence of events associated with the fluctuations in the intensity of the transverse circulation. This hydrodynamical process could also explain the elevated values of nutrients related to a plume of water in the same region by Greisman and Ingram (1977) during a neap tide cruise. This "trapping" of the water mass was also observed in our study during the neap tide.

The observations of Vézina *et al.* (1995), made in the same area over two spring-neap cycles the preceeding year (1989), were also consistent with our circulation pattern. Although there were differences in the circulation dynamics between the two years, the establishment of a cross-shore front between fresher waters along the south shore and saltier waters offshore was associated with increases in phytoplankton biomass during the summer bloom period in 1989 and in 1990. The rapid mesoscale variations in the distribution of phytoplankton can be due to a switch from an outflow to a recirculating regime as well as by fluctuations in the intensity of the transverse current and its associated eddies. During the 1989 cruise, the establishment of a cross-shore front was also consistent with a strong transverse current set up this time by a pulse of upwelled waters in the northwest corner. Evidence of the trapping of a bloom was observed during the 1989 cruise in the same area where the trapping was observed in 1990 during the neap cruise.

*f. A new conceptual model to explain the mesoscale variability in the LSLE*

Mesoscale features in production in the LSLE have been described by Therriault and Levasseur (1985). They identified three zones converging in our study area over an annual scale: (1) an outflow zone along the south shore shallows with the lowest salinities and the lowest productivity on average; (2) an upwelling zone overlying the Laurentian Channel

with the highest salinities and moderate productivity; and (3) a plume zone over the downstream part of the LSLE with intermediate salinities and the highest production levels. The differences in productivity were attributed to separate physical characteristics of these zones: high turbidity, strong currents, and vertical mixing that limit light availability in the outflow zone; low vertical stability that limits photosynthetic efficiency and the utilization of nutrients in the upwelling zone; and increased vertical stability in the plume zone provided by freshwater runoff from the north shore rivers that allows higher efficiency in the utilization of nutrients advected from the upwelling zone. In arriving at their classification, these authors averaged out the spatio-temporal variability at smaller temporal and spatial scales, which they noted was very large.

Based on the above discussion, we propose a different conceptual model in the LSLE that emphasizes interactions among water masses as opposed to their individual characteristics. Since the highest salinities were measured in the north shore region and the discharge of the north shore rivers decreased during the study period, we propose that the plume zone along the north shore is largely stabilized not by the runoff from the north shore rivers but by the cross-shore transport of pulse waters from the south to the north shore (mixing between south brackish waters and north upwelling waters in 1989 or runoff from the St. Lawrence and Saguenay rivers in 1990). We also submit that the intensity of the transverse current may fluctuate over time scales of 3–5 days in relation to the passage of freshwater pulses from the mouth of the Saguenay to the Rimouski region. The strength and therefore the signature of these pulses may be enhanced by the neap-spring tidal mixing near the mouth of the estuary. This variability seems to cause changes in phytoplankton blooms and distributions in the LSLE. The injection of buoyancy and the vertical stability from the south shore could have an impact on the toxic algal blooms that are known to develop along the north shore, mainly within the combined plume of the Manicouagan and Outardes rivers that extends into a permanent surface coastal jet, the Gaspé Current, flowing seaward around the Gaspé Peninsula toward the Magdalen Shallows (Therriault *et al.*, 1985; Turgeon *et al.*, 1990). The atmospheric or oceanographic processes that control these fluctuations must still be elucidated.

*Acknowledgments.* This work was supported by a team grant from FCAR (Formation de Chercheurs et Aides à la Recherche de Québec, Ministère de l'Education et de l'Enseignement Supérieur du Québec), the Natural Sciences and Engineering Research Council of Canada, Fisheries and Oceans Canada, and the University of Québec at Rimouski. This paper is a contribution to the programs of the Maurice Lamontagne Institute (Ocean Productivity Division, Department of Fisheries and Oceans, Canada) and of the Oceanographic Centre of Rimouski. We acknowledge the help of D. Blasco, A. Tremblay, S. Arsenault, G. Desmeules, P. Vinet, C. Bélanger, and C. Brassard for technical assistance. The ADCP was lent to us by Dr. R. F. Marsden of the Royal Roads Military College. Our sincere appreciation goes to the excellent crew of the M. V. *Alcide C. Horth* and to the Maritime Institute of Rimouski for their logistic support. We appreciate the help of J. Noël and C. Lafleur who kindly provided the final figures. Gratitude is extended to L. Devine for reading the manuscript and offering comments.

## REFERENCES

Aminot, A. and M. Chaussepied. 1983. Manuel des analyses chimiques en milieu marin, CNEXO, Brest, 395 pp.

Anderson, J. J. and A. Okubo. 1982. Resolution of chemical properties with a vertical profiling pump. Deep-Sea Res., *29,* 1013–1019.

Angel, M. V. and M. J. R. Fasham. 1983. Eddies and biological processes, *in* Eddies in Marine Science, A. R. Robinson, ed., Springer-Verlag, Berlin, 492–524.

Bertine, K., J. K. Cochran, L. E. Cronin, W. P. Davis, C. S. Martens, L. R. Pomeroy, J. J. Schubel, J. G. Taft, J. Teal and R. Wilson. 1979. Estuaries, *in* Workshop on Assimilative Capacity of U.S. Coastal Waters for Pollutants, Cristal Mountain, Washington, July 29–August 4, 1979, E. D. Goldberg, ed., National Oceanic and Atmospheric Administration Environmental Research Laboratories, Boulder, Colorado, 59–97.

Blasco, D. 1971. Composición y distribución del fitoplancton en la región de afloramiento de las costas peruanas. Investigación Pesquera, *35,* 61–112.

Boynton, W. R., W. M. Kemp and C. W. Keefe. 1982. A comparative analysis of nutrients and other factors influencing estuarine phytoplankton, *in* Estuarine Comparisons, V. S. Kennedy, ed., Academic Press, New York, N.Y., 69–90.

Cloern, J. E. 1984. Temporal dynamics and ecological significance of salinity stratification in an estuary (South San Francisco Bay, USA). Oceanol. Acta, *7,* 137–141.

—— 1987. Turbidity as a control on phytoplankton biomass and productivity in estuaries. Cont. Shelf Res., *7,* 1367–1381.

—— 1991. Tidal stirring and phytoplankton bloom dynamics in an estuary. J. Mar. Res., *49,* 203–221.

Cloern, J. E., T. M. Powell and L. M. Huzzey. 1989. Spatial and temporal variability in South San Francisco Bay (USA). II. Temporal changes in salinity, suspended sediments, and phytoplankton biomass and productivity over tidal time scales. Estuar. Coast. Shelf Sci., *28,* 599–613.

Demers, S., P. E. Lafleur, L. Legendre and C. L. Trump. 1979. Short-term covariability of chlorophyll and temperature in the St. Lawrence Estuary. J. Fish. Res. Board Can., *36,* 568–573.

Demers, S. and L. Legendre. 1981. Mélange vertical et capacité photosynthétique du phytoplancton estuarien (Estuaire du Saint-Laurent). Mar. Biol., *64,* 243–250.

Deutsch, C. V. and A. G. Journel. 1992. GSLIB—Geostatistical Software Library and User's guide, Oxford University Press, New York, 340 pp.

El-Sabh, M. I. 1977. Circulation pattern and water characteristics in the lower St. Lawrence Estuary, *in* Symposium on Modelling of Transport Mechanisms in Oceans and Lakes, T. Murty, ed., Mar. Sci. Directorate, M. S. Rep., *43,* 243–248.

Fisher, T. R., L. W. Harding Jr., D. W. Stanley and L. G. Ward. 1988. Phytoplankton, nutrients, and turbidity in the Chesapeake, Delaware, and Hudson estuaries. Estuar. Coast. Shelf Sci., *27,* 61–93.

Forrester, W. D. 1967. Currents and geostrophic currents in the St. Lawrence Estuary. Bedford Inst. Oceanogr., Rep. Ser., *67–5,* 175 pp.

—— 1970. Geostrophic approximation in the St. Lawrence estuary. Tellus, *1,* 53–65.

—— 1974. Internal tides in the St. Lawrence Estuary. J. Mar. Res., *32,* 55–66.

Franks, P. J. S. 1992. Phytoplankton blooms at fronts: patterns, scales, and physical forcing mechanisms. Rev. Aquat. Sci., *6,* 121–137.

Freeland, H. J., F. M. Boland, J. A. Church, A. J. Clarke, A. M. G. Forbes, A. Huyer, R. L. Smith, R. O. R. Y. Thompson and N. J. White. 1986. The Australian Coastal Experiment: a search for coastal-trapped waves. J. Phys. Oceanogr., *16,* 1230–1249.

Gill, A. E. 1982. Atmosphere-Ocean Dynamics, Academic Press, New York, 662 pp.

Gratton, Y., G. Mertz and J. A. Gagné. 1988. Satellite observations of tidal upwelling and mixing in the St. Lawrence Estuary. J. Geophys. Res., *93,* 6947–6954.

Greisman, P. and R. G. Ingram. 1975. Physical processes bearing upon the productivity in the St. Lawrence Gulf-Estuary system. Atmosphere, Spec. Issues, 9th Annu. Congr. Can. Meteorol. Soc., *13,* 36 (Abstract only).

—— 1977. Nutrient distribution in the St. Lawrence Estuary. J. Fish. Res. Board Can., *34,* 2117–2123.

Harrison, P. J., P. J. Clifford, W. P. Cochlan, K. Yin, M. A. St. John, P. A. Thompson, M. J. Sibbald and L. J. Albright. 1991. Nutrient and plankton dynamics in the Fraser River plume, Strait of Georgia, British Columbia. Mar. Ecol. Prog. Ser., *70,* 291–304.

Hartigan, J. A. 1975. Clustering Algorithms, John Wiley and Sons, Inc., N.Y.

Huzzey, L. M., J. E. Cloern and T. M. Powell. 1990. Episodic changes in lateral transport and phytoplankton distribution in south San Francisco Bay. Limnol. Oceanogr., *35,* 472–478.

Ingram, R. G. 1975. Influence of tidal-induced vertical mixing on primary productivity in the St. Lawrence Estuary. Mem. Soc. R. Sci. Liege, *6,* 59–74.

—— 1979. Water mass modification in the St. Lawrence Estuary. Naturaliste can., *106,* 45–54.

Ingram, R. G. and M. I. El-Sabh. 1990. Fronts and mesoscale features in the St. Lawrence Estuary, *in* Oceanography of a Large-Scale Estuarine System, The St. Lawrence, M. I. El-Sabh and N. Silverberg, eds., Springer-Verlag, New York, N.Y., Coast. Estuar. Stud. *39,* 71–93.

Koutitonsky, V. G., R. E. Wilson and M. I. El-Sabh. 1990. On the seasonal response of the lower St. Lawrence Estuary to buoyancy forcing by regulated river runoff. Estuar. Coast. Shelf Sci., *31,* 359–379.

Laforêt, R. G. 1994. Oceanographic and acoustic implications of freshwater releases into the Laurentian Channel. M. Sc. Thesis, Royal Roads Military College, Victoria, B.C., 95 pp.

Legendre, L. and S. Demers. 1985. Auxiliary energy, ergoclines and aquatic biological production. Naturaliste can., *112,* 5–14.

Levasseur, M., J.-C. Therriault and L. Legendre. 1984. Hierarchical control of phytoplankton succession by physical factors. Mar. Ecol. Prog. Ser., *19,* 211–222.

Lund, J. W. G., C. Kipling and E. D. Lecren. 1958. The inverted microscope method of estimating algal numbers and the statistical basis of estimations by counting. Hydrobiologia, *11,* 143–170.

Malone, T. C., W. M. Kemp, H. W. Ducklow, W. R. Boynton, J. H. Tuttle and R. B. Jonas. 1986. Lateral variation in the production and fate of phytoplankton in a partially stratified estuary. Mar. Ecol. Prog. Ser., *32,* 149–160.

Marcotte, D. 1991. Cokriging with Matlab. Computers and Geosciences, *19,* 1265–1280.

MATLAB 1992. MATLAB Reference Guide, The Math Works, Inc., Natick, Massachusetts, 548 pp.

Mertz, G., M. I. El-Sabh and V. G. Koutitonsky. 1989. Low frequency variability in the Lower St. Lawrence Estuary. J. Mar. Res., *47,* 285–302.

Mertz, G. and Y. Gratton. 1990. Topographic waves and topographically induced motions in the St. Lawrence Estuary, *in* Oceanography of a Large-Scale Estuarine System, The St. Lawrence, M. I. El-Sabh and N. Silverberg, eds., Springer-Verlag, New York, N.Y., Coast. Estuar. Stud., *39,* 94–108.

Monbet, Y. 1992. Control of phytoplankton biomass in estuaries: a comparative analysis of microtidal and macrotidal estuaries. Estuaries, *15,* 563–571.

Murty, T. S. and M. I. El-Sabh. 1977. Transverse currents in the St. Lawrence Estuary: a theoretical treatment, *in* Transport Processes in Oceans and Lakes, R. J. Gibbs, ed., Plenum Press, New York, N.Y., 35–62.

Nixon, S. W. and M. E. Q. Pilson. 1983. Nitrogen in estuarine and coastal marine ecosystems, *in* Nitrogen in the Marine Environment, E. J. Carpenter and D. G. Capone, eds., Academic Press,

New York, N.Y., 563–648.

Parsons, T. R., Y. Maita and C. M. Lalli. 1984. A manual of chemical and biological methods for seawater analysis, Pergamon Press, N.Y., 173 pp.

Queguiner, B. and P. Treguer. 1986. Freshwater outflow effects in a coastal, macrotidal ecosystem as revealed by hydrological, chemical, and biological variabilities (Bay of Brest, Western Europe), *in* The Role of Freshwater Outflow in Coastal Marine Ecosystems, S. Skreslet, ed., NATO ASI Series-Series G. Ecological Sciences, *7,* Springer-Verlag, Berlin, 219– 230.

Savenkoff, C., J.-P. Chanut, A. F. Vézina and Y. Gratton. 1995a. Distribution of biological activity in the lower St. Lawrence Estuary as determined by multivariate analysis. Estuar. Coast. Shelf Sci., *40,* 647–664.

Savenkoff, C., A. F. Vézina, J.-P. Chanut and Y. Gratton. 1995b. Respiratory activity and $CO_2$ production rates of microorganisms in the lower St. Lawrence Estuary. Cont. Shelf Res., *15,* 613–631.

Sinclair, M. 1978. Summer phytoplankton variability in the lower St. Lawrence Estuary. J. Fish. Res. Board Can., *35,* 1171–1185.

Sinclair, M., D. V. Subba Rao and R. Couture. 1981. Phytoplankton temporal distributions in the estuaries. Oceanol. Acta, *4,* 239–246.

Strickland, J. D. H. and T. R. Parsons. 1972. A Practical Handbook of Seawater Analysis, 2nd ed., Fisheries Research Board of Canada, Ottawa, 310 pp.

Tee, K.-T. and T.-H. Lim. 1987. The freshwater pulse-a numerical model with application to the St. Lawrence Estuary. J. Mar. Res., *45,* 871–909.

Therriault, J.-C. and G. Lacroix. 1976. Nutrients, chlorophyll, and internal tides in the St. Lawrence Estuary. J. Fish. Res. Board Can., *33,* 2747–2757.

Therriault, J.-C. and M. Levasseur. 1985. Control of phytoplankton production in the lower St. Lawrence Estuary: light and freshwater runoff. Naturaliste can., *112,* 77–96.

Therriault, J.-C., J. Painchaud and M. Levasseur. 1985. Factors controlling the occurrence of *Protogonyaulax tamarensis* and shellfish toxicity in the St. Lawrence Estuary: freshwater runoff and the stability of the water column, *in* Toxic Dinoflagellates, D.M. Anderson, A.W. White and D.G. Baden, eds., Elsevier Science Publishing Co., Inc., New York, N.Y., 141–146.

Turgeon, J., A. D. Cembella, J.-C. Therriault and P. Béland. 1990. Spatial distribution of resting cycts of *Alexandrium* spp. in sediments of the lower St. Lawrence Estuary and the Gaspé coast (eastern Canada), *in* Toxic Marine Phytoplankton, E. Granéli, B. Sundström, L. Edler and D. M. Anderson, eds., Proceedings of the Fourth International Conference on Toxic Marine Phytoplankton, held June 26–30, 1989, in Lund, Sweden, Elsevier Science Publishing Co., Inc., New York, N.Y., 238–243.

Vézina, A. F., Y. Gratton and P. Vinet. 1995. Mesoscale physical-biological variability during a summer phytoplankton bloom in the lower St. Lawrence Estuary. Estuar. Coast. Shelf Sci., *41,* 393–411.

Wafar, M. V. M., P. Le Corre and J. L. Birrien. 1989. Transport of carbon, nitrogen and phosphorus in a Brittany river, France. Estuar. Coast. Shelf Sci., *29,* 489–500.

Wilkinson, L. 1992. Systat for Windows: Statistics, Version 5 Edition, Systat, Inc., Evanston, IL, 750 pp.

Received: *11 December, 1995;* revised: *1 August, 1996.*